Compressive Sensing-Based Three-Dimensional Laser Imaging With Dual Illumination

YULONG AN[1], **YANMEI ZHANG**[1], **HAICHAO GUO**[1,2], **AND JING WANG**[1]

[1]Beijing Institute of Technology, Beijing 100081, China
[2]China Academy of Space Technology, Beijing 100081, China

Corresponding author: Yanmei Zhang (zhangym0726@163.com)

ABSTRACT Low-cost 3D imaging, particularly by using laser detection and ranging (LIDAR), is important for applications such as object recognition, surface mapping, and machine vision. Conventional time-of-flight LIDAR uses a scanned laser to obtain the intensity and range of targets, which requires a narrow bandwidth of illumination and high-speed synchronizers. This paper presents a nonscanning prototype of a pulse-width-free 3D LIDAR which combines single-pixel imaging and diffractive optical elements, for the first time to our knowledge. Compressive sensing techniques are used to measure echo pulses from the target and reconstruct the intensity map of the target scene. Diffractive optical elements are also applied to generate structured illumination and the depth map of the target scene can be obtained from laser spot extraction. The simulation results are presented to verify the effectiveness of the proposed prototype as well as illustrate its superiority where traditional 3D imaging methods are unavailable or limited. This novel prototype has advantages of low cost and flexible structure at wavelengths beyond the visible spectrum and will be highly interesting for practical applications.

INDEX TERMS Compressed sensing, image reconstruction, infrared imaging, laser radar.

I. INTRODUCTION

Laser detection and ranging (LIDAR) is a surveying method for measuring the reflectivity and range of a target scene by illuminating it with a pulsed laser and receiving the reflected pulses with a sensor [1]. LIDAR is widely used in target detection and recognition, computer vision and three-dimensional (3D) scene imaging since it has the merits of high reliability, longitudinal resolution and anti-electromagnetic interference ability. In particular, non-scanning LIDAR systems have been greatly developed in recent years due to its low complexity, detection ability of moving target and imaging obscuring targets [2]–[5].

In general, single-pixel nonscanning LIDAR is achieved by employing a new sensing technology named compressive sensing (CS), combining sampling and compression into a single nonadaptive linear measurement process [6]–[9]. Candès and Wakin [10] and Donoho [11] first proposed the CS theory which is a major breakthrough for signal acquisition theory. CS theory assumes that the spectrum of a signal in a selected transform has only a few nonzero components.

By means of convex optimization in the selected transform domain, one can recover certain signals and images from far fewer samples. The CS framework has expanded greatly from methodology to applications in active imaging after Duarte and Davenport presented a signal-pixel imaging camera that can operate efficiently based on a digital micromirror device (DMD) [12], [13]. In terms of range estimation, time-of-flight (TOF) techniques are widely used by correlating the detection time of the back-scattered light with the time of illumination pulse [14], [15]. Howland *et al.* [16], [17] combined CS theory with a TOF photon counting LIDAR configuration where transverse spatial resolution is obtained without scanning. Via optical multiplexing, Li *et al.* [18] proposed a CS-TOF imaging architecture which achieved significant improvement in spatial resolution for natural scene. Although these frameworks provide simple and low-cost solutions compared with conventional TOF LIDAR, the range resolution of the systems depends on narrow bandwidth of illumination laser pulses and comparative detectors. By applying indirect ranging methods to overcome these limitations, various achievements have been made. Li *et al.* [19] presented a prototype of gated viewing laser imaging with CS where the 3D scene can be reconstructed by the time-slicing (TS) technique. Gao

The associate editor coordinating the review of this manuscript and approving it for publication was Zhaoqing Pan.

et al. [20] proposed a super-resolution algorithm to acquire range information of space-continuous targets based on CS theory and multihypothesis prediction. In addition, range information can be obtained by analyzing the intensity correlation in the overlapping areas of two range gated, thanks to narrow rectangular-shaped or triangular-shaped pulses generated by costly and complicated illuminator [21].

Structured illumination generated by diffractive optical elements (DOEs) is also common in 3D imaging systems. There is one special kind of DOEs named Dammann grating which was first proposed by Dammann and Görtler [22] with obvious advantages such as low cost, low power consumption and small size. Dammann grating can split one laser beam into a predesigned beam array where energy of each beam is equal. Several outstanding 3D imaging efforts with Dammann grating have received extensive attraction recently [23]. For example, Wei proposed a binocular camera to construct 3D profilometry and then proposed a colorful 3D imaging method using near-infrared laser [24], [25].

In this paper, a prototype of CS based nonscanning LIDAR with general illumination and structured illumination is proposed. The prototype combines the single-pixel camera technology with the diffractive optical elements. Laser pulses are emitted toward the target and then the scattered light from the target returns to the system. Peak values of the total echo pulses are recorded for reconstructing the range-intensity profile which consists of a depth map and an intensity map. On the one side, the depth map of the target can be estimated based on laser spot extraction by structure illumination. On the other side, the intensity map of the target can be recovered by either integral sparse sampling or complementary sparse sampling by uniform illumination. The novel solution to the ranging problem in 3D LIDAR imaging lies in the proposed prototype that can overcome the limitation imposed by hardware, by depending on numerical processing power. Numerical simulations for 3D imaging with various subrates are presented to demonstrate the performance of the proposed prototype.

This paper is organized as follows. Section 2 reviews CS theory and its reconstruction model. Section 3 presents a prototype of the dual illumination LIDAR and its mathematical model. Section 4 presents the 3D reconstruction method to estimate the depth map and recover the intensity map. Section 5 shows simulation experiments which are carried out to validate the proposed prototype. Finally, Section 6 is the conclusion.

II. COMPRESSIVE SENSING

CS techniques have previously designed to use prior knowledge to determine original signals from significantly reduced measurements compared with conventional sampling [26]–[28]. To be more specific, the goal of CS is to recover the signal vector $x \in \mathbb{R}^n$ from the measurements vector

$$y = \Phi x \qquad (1)$$

where an $m \times n$ measurement matrix Φ (such that $m \ll n$) is prearranged. The subsampling rate is defined by $subrate = m/n$ and general recover method is incapable since $subrate \ll 1$.

According to CS theory, signals have a sparse representation by some linear transform coding in terms of the coefficients $\{\alpha_i\}$ of an orthonormal basis expansion $x = \sum_{i=1}^{n} \alpha_i \psi_i$ where $\{\psi_i\}_{i=1}^{n}$ are the $n \times 1$ basis vectors. Let $x = \Psi\alpha$, where the $n \times n$ transforming matrix Ψ is the stack of vectors $\{\psi_i\}_{i=1}^{n}$ as columns and α is a sparse coefficient vector. For natural images, finding a good transform has been studied extensively and notable achievements such as discrete cosine transform (DCT) and discrete wavelet transform (DWT) are widely used.

Then, the reconstruction of x is synthesized by recovering $\hat{\alpha}$ and processing the mathematics problem: $\hat{x} = \Psi\hat{\alpha}$. $\hat{\alpha}$ is recovered by solving the convex optimization problem:

$$\hat{\alpha} = \arg\min_{\alpha} \|\alpha\|_0 \quad s.t. \ y = \Phi\Psi\alpha \qquad (2)$$

where $\|\cdot\|_0$ is the l_0-norm that counts the number of nonzero entries of α and can be transformed into either l_1-norm or l_2-norm by convex relaxation techniques.

Various CS algorithms have been developed to tackle this kind of inverse problems and the exact recovery of x is guaranteed by solving the problem with total variation (TV) regularization [29]. The TV minimization based on augmented lagrangian and alternating direction algorithms (TVAL3) scheme is able to handle different boundary conditions for α and is widely used as the reconstruction algorithm in CS systems [30].

III. SYSTEM DESCRIPTION

The prototype of a pulse-width-free LIDAR with dual illumination is illustrated in Fig. 1. It combines classical single-pixel imaging framework with two laser transmitters where one of them is with DOEs. As is shown in Fig. 1, the prototype mainly consists of two transmitters, a camera lens as the receiver, a narrowband filter (NBF), a beam splitter, a digital micromirror device (DMD), a series of focus lens, a one-pixel avalanche photodiode (APD) detector and a PC. There is red light path with white arrows and orange data path in dotted line. One of the transmitters emits flat-top Gaussian beam and uniform beam illuminates the integral scene. In the other transmitter, a near-infrared (NIR) Dammann grating is embedded in the projection unit and output laser beam is split into dot array to illuminate the scene. The beam splitter is used for changing the propagation direction of light and avoiding apparent focus error on DMD. First, one transmitter emits laser beam toward the target scene. Second, reflected light returns to the system collecting by the camera lens. Third, a DMD is applied to conduct spatial modulation shown as a series of 0-1 patterns defined beforehand. Forth, a narrowband filter is used to remove background radiation from sunlight and other sources and the reflected light arrives at the one-pixel APD detector. When the other
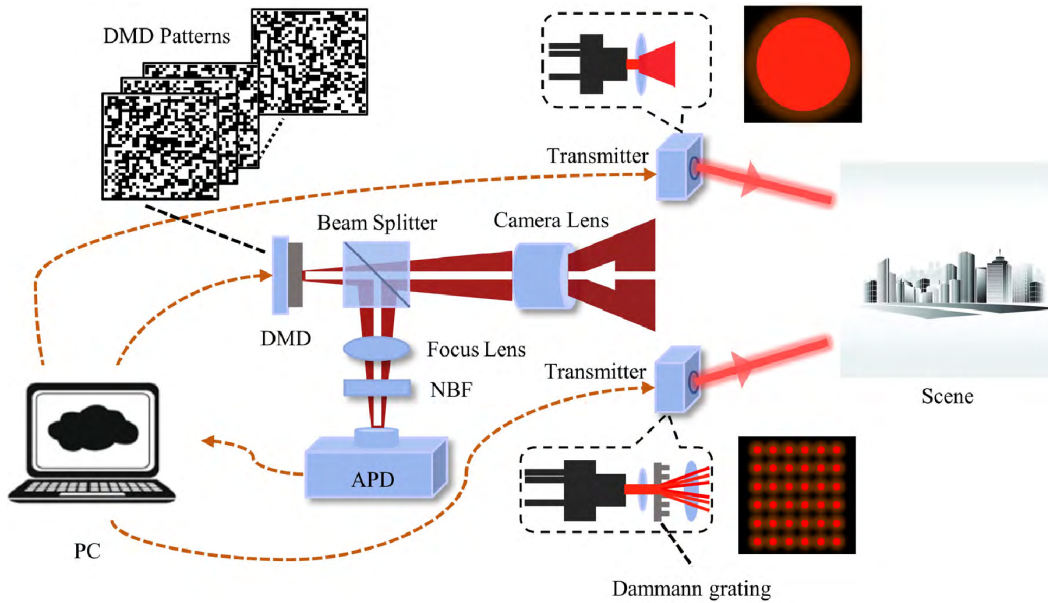
FIGURE 1. Schematic of dual illumination compressive LIDAR.

transmitter works, the system perform the same modulation and sampling procedure. Throughout the whole prototype, no temporal modulation of structure light and reflected light is needed during measurements which is quite novel in 3D laser imaging.

To generate structured light, the illuminator with Dammann grating is an important part in the whole prototype. Two-dimensional (2D) Dammann grating is capable to split most of the illumination power into a desired diffractive spot matrix with equal intensity as is shown in Fig. 2. The spot pattern has the advantage of high brightness and high compression ratio. According to diffraction theory, the structured light is a rectangular dot matrix by $m_x \times m_y$ dots and the original half divergence angle is

$$\theta_m = \arcsin \frac{(m-1)\lambda}{d_0}, \quad m = m_x, \ m_y \tag{3}$$

where m is even, λ is the wavelength of laser and d_0 is the period of the Dammann grating. Generally, the output divergence angle θ of the transmitter is extended by a lens and modulated by grating fabrication. We can have the area of each diffractive spot A as a function of the range to reference plane R by theoretical derivation:

$$A = \pi R^2 \tan^2 \theta \tag{4}$$

To be more specific, the system model is presented as follows. The time propagation and pulse energy distribution U in 3D space from the transmitter is of the form:

$$U(a, b, t) = I_0 \cdot I(a, b) \cdot p_t(t) \tag{5}$$

where I_0 is the total power constant of the laser pulse, (a, b) represents a particular position under rectangular coordinate system perpendicular to the direction of laser propagation,

$I(a, b)$ is the normalized function for special distribution of the pulse and $p_t(t)$ is the normalized function for time propagation of the pulse. Moreover, $p_t(t)$ is represented as:

$$p_t(t) = \begin{cases} (t/\tau)^2 \, e^{\left(-\frac{t}{\tau}\right)} & t \geq 0 \\ 0 & t < 0 \end{cases} \tag{6}$$

where $\tau = T_{1/2}/3.5$ and $T_{1/2}$ is the full width at half maximum (FWHM) of the pulse. Assuming that the target is a Lambert diffuse point-like reflector, the power of the echo signal P_r can be represented as the following formula:

$$P_r(R) = \frac{I_0 I(a, b) \, \tau_t \tau_r \tau_a^2 \rho \cos \beta}{\pi \, \Omega_t R^4} \tag{7}$$

where τ_t and τ_r are the efficiencies of the optical transmitting and receiving systems, respectively; τ_α is the single-pass atmospheric transmittance; ρ is the reflectance of the target; β is the angle between the detecting direction and the normal of the Lambert surface; Ω_t is the scattering solid angle of target in steradians and R is the range between the target and the receiver [31].

Then the range-discretized form of the total power of echo pulses by sparse sampling in the view of field can be described as a sum of pulse from each pixel with different amplitudes and delay times:

$$p_{r,j}(t) = \sum_i^n \Phi_{(j,i)} P_r(R_i) \, p(t - t_i) \tag{8}$$

where $t_i = 2R_i/c$ and c is the speed of light and Φ is the CS measurement matrix.
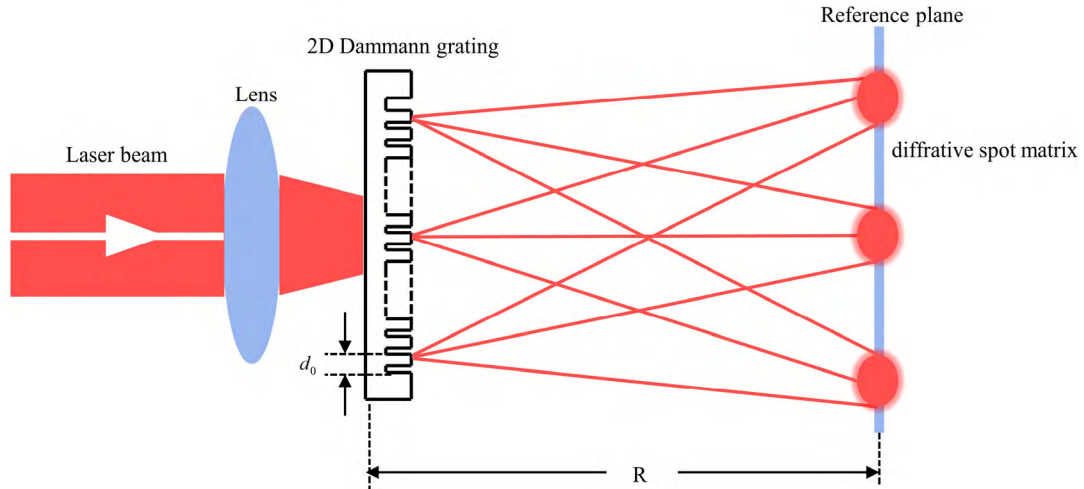
FIGURE 2. Generation of a diffractive spot matrix with a 2D Dammann grating.

IV. 3D RECONSTRUCTION METHOD

For 3D compressive imaging, a 2D extended mathematical model of measuring process is presented as follows according to formula (8) in a discretized matrix form:

$$Y = \Phi E \tag{9}$$

where Φ is a measurement matrix, E is a $n \times l$ matrix with $n = p \times q$ and Y is a $m \times l$ matrix as total echo waveform. The target scene is supposed to be recovered as an intensity map with a transverse resolution $p \times q$. The ith row of E $(i = 1, 2, \cdots n)$ represents the echo pulse from the scene corresponding to the ith pixel on DMD and the jth row of Y $(i = 1, 2, \cdots m)$ represents the total echo pulse with jth DMD pattern's modulation recorded by the detector.

The task of 3D imaging is to determine a range value and a gray value for each pixel in the target scene. This section presents a depth map estimation method and alternative intensity map reconstruction methods to achieve 3D imaging in CS framework.

A. DEPTH MAP ESTIMATION

However, only peak values of the total echo pulses are required to recover the intensity information in CS framework rather than recording the whole waveform. In this instance, we define vector $y = (y_1, y_2, \cdots y_m)^T$ as the measurements when the transmitter with Dammann grating embedded illuminates the target scene, diagonal matrix $I \in \mathbb{R}^{n \times n}$ as the discretized intensity distribution matrix of the diffractive spot and vector $x = (x_1, x_2, \cdots x_n)^T$ as the original gray values of pixels in the target scene. The sampling process is modeled as follows:

$$y = \Phi I x = \Phi x' \tag{10}$$

where $x' = Ix$ depends on associative in matrix product.

Firstly, we enforce the sparsity of x' in some domains as a prior and solve the l_2-regularzied non-negativity

constrained inverse problem:

$$\hat{x}_c = \arg\min_{x_c} \|D_i x_c\|_2 + \frac{\mu}{2} \|\Phi_c x_c - y_c\|_2^2, \quad s.t. \ x_c \geq 0 \tag{11}$$

where $D_i x' \in \mathbb{R}^2$ is the discrete gradient of x' at pixel i, by TVAL3 solver with default setting μ. Then, the recovered distribution matrix of diffractive spot $\hat{I}$ can be estimated by proper threshold operation considering that there is no echo pulse if there is no laser spot on the target. Finally, a $s \times s$ depth map $\hat{d}$, which is consistent with the beam-splitting ratio of Dammann grating, is generated based on block-wise estimation. The recovered signal $\hat{I} \in \mathbb{R}^{n \times 1}$ is reshaped into a $p \times q$ matrix and then split into a series of $s \times s$ blocks with the size of $(p/s) \times (q/s)$. The value of each pixel in $\hat{d}$ is estimated depending on the intensity distribution in each block, respectively.

B. INTENSITY MAP RECONSTRUCTION BY INTEGRAL SPARSE SAMPLING

Intensity map shows the gray value of the object obtained by transmitting and reflecting laser pulses. When the transmitter with Dammann grating embedded works, the intensity information obtained by the prototype is from some, but not all, pixels of the target scene. To achieve integral imaging, a procedure of sparse sampling and reconstruction, which is called integral sparse sampling (ISS) for the sake of comparison with another procedure, is carried out with the transmitter emitting flat-top Gaussian beam and illuminating the whole target scene. The procedure is similar to typical compressive single-pixel LIDAR that combines pattern projection and single-pixel detector to reconstruct intensity map $\hat{x}$.

C. INTENSITY MAP RECONSTRUCTION BY COMPLEMENTARY SPARSE SAMPLING

Since a considerable part of gray values of the pixels are obtained when the transmitter with Dammann grating works,
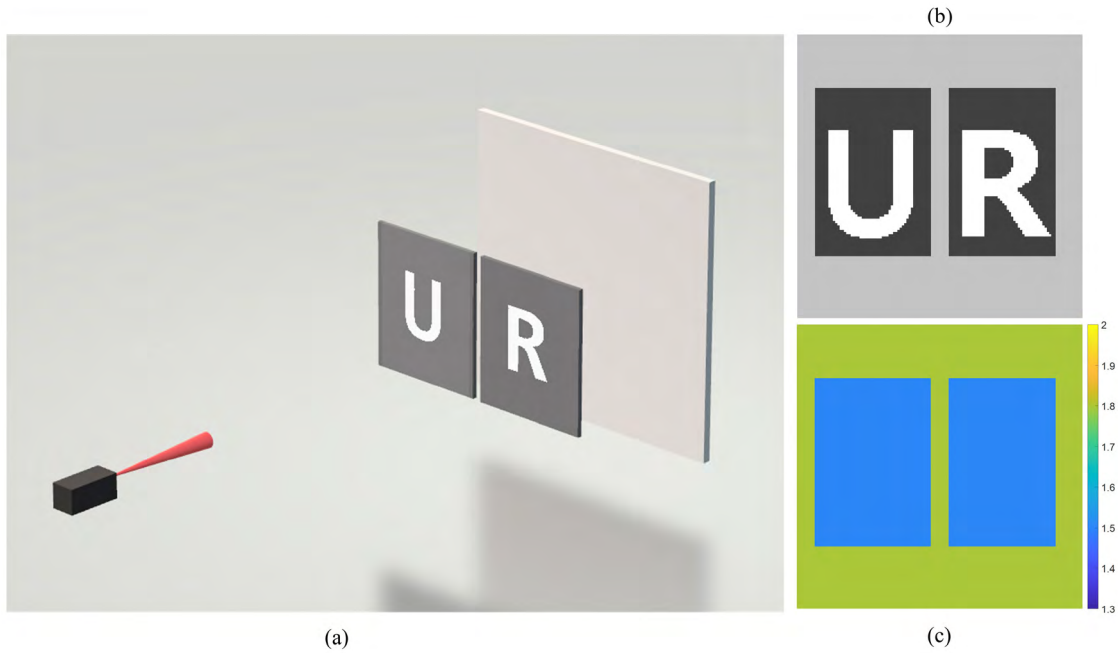
FIGURE 3. 3D scene ranged from 1.50 m to 1.80 m. (a) is the conceptual graph of the target; (b) and (c) are the original range-intensity profiles; (b) is the original intensity map; (c) is the original depth map.

we only need sample the echo pulses from the missed pixels and reconstruct the integral intensity map $\hat{x}$ based on the existing pixels in $\hat{x}'$. This procedure is called complementary sparse sampling (CSS) and the number of measurements can be significantly reduced comparing with ISS. Depending on $\hat{x}'$ and $\hat{I}'$, the original gray value of the target x can be divided into two vectors $x_d \in \mathbb{R}^{n_d \times 1}$ and $x_c \in \mathbb{R}^{n_c \times 1}$ which are measured and reconstructed respectively. x_d represents the pixels that are capable to be recovered as a byproduct of depth map estimation in x and x_c represents the pixels that is going to be reconstructed by CSS in x respectively. For convenience, the results of optimization reconstruction are denoted as $\hat{x}_d$ and $\hat{x}_c$ accordingly. CSS is carried out with the transmitters emitting flat-top Gaussian beam which illuminates the whole target scene and modeled as:

$$y_c = \Phi'_c x \tag{12}$$

where Φ'_c is a $m_c \times n$ measurement matrix with some specific all-zero columns and y_c is the CSS vector. A proven and universal measurement matrix $\Phi_c \in \mathbb{R}^{m_c \times n_c}$ is revealed if we omit the specific all-zero columns in Φ'_c. Therefore, we apply TVAL3 solver with default settings to solve the inverse problem:

$$\hat{x}_c = \arg\min_{x_c} \|D_i x_c\|_2 + \frac{\mu}{2}\|\Phi_c x_c - y_c\|_2^2, \quad s.t. \ x_c \geq 0. \tag{13}$$

$\hat{x}$ is finally obtained combining $\hat{x}_d$ and $\hat{x}_c$.

In total, the reconstructed 3D image of the target scene can be achieved as a combination of an intensity map $\hat{x}$ and a depth map $\hat{d}$.

V. SIMULATION RESULTS AND DISCUSSION

In this section, a simulation system is established and the simulation results are presented to validate the effectiveness of the proposed prototype and the pulse-width-free 3D active imaging method. The numerical simulations are done with CPU of Intel Core i3-3220 and 4.00GB RAM by matlab 2016a (64bits). The pulsed laser works at low repetition rate, high pulse energy to illuminate the target scene and a 32×32 array illuminator with Dammann grating embedded are carried out for depth estimation as well. A series of DMD patterns derived from 2D Hadamard transform are used to modulate the echo pulses for CS measurements [18]. The main parameters of the LIDAR system are given in Table 1. Generally, the range resolution of TOF compressive LIDAR with similar parameters is about 6 meters. The proposed prototype can provide range super-resolution ability if we use it as the standard.

As is shown in Fig. 3 (a), a 3D scene is designed as the target which consists of two square cardboards with letters 'U' and 'R' printed on and a white cardboard as the back-ground. This is a typical target scene in CS-based 3D imaging [16], [17], [32], [33]. The boards are distinguished and located parallelly towards the imaging system. The distance between the imaging system and the cardboard with 'U' is 1.50 m and so is the distance between the imaging system and the cardboard with 'R'. The distance between the imaging system and the background is 1.80 m. The 3D scene is modeled by a combination of two matrixes, which are shown as the intensity map in Fig. 3 (b) and the depth map in Fig. 3 (c). The intensity map shows the reflectivity distribution of the target and the depth map shows the distance
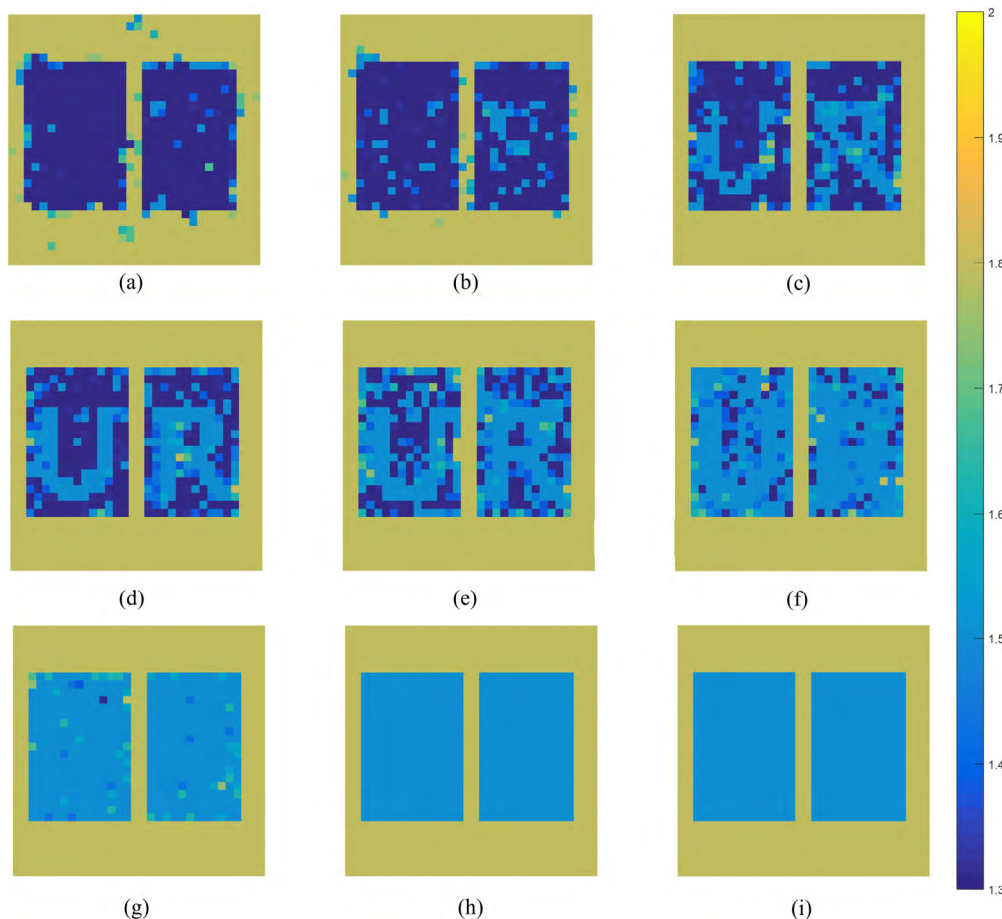
FIGURE 4. Visual comparison of the estimated depth maps of the target scene with various subrates (from 4% to 36%) in the absence of noise. From left to right and top to bottom: the subrate increases successively by 4%.

TABLE 1. Parameters of the simulation experiments.

Expression	Value
Wavelength	905 nm
Sampling Rate of APD	500 MHz
Peak Power of Transmitter Pulse	70 W
FWHM	40 ns
Splitting ratio of Dammann grating	32×32
Efficiency of Optical Transmitting System	0.9
Efficiency of Optical Receiving System	0.9
Single-pass Atmospheric Transmittance	0.98

FIGURE 5. NMSE for estimated depth map with various subrates.

(in pixels) between the target and the imaging system. Colors correspond to the value of the estimated depth and a bar on the right side is added as an annotation.

Fig. 4 illustrates the visual comparison of the estimated depth maps of the target scene by the proposed prototype with various subrates from 4% to 36% in the absence of noise. When the target is illuminated by the transmitter with Dammann grating embedded, an intensity map of the target is reconstructed with high quality owing to the effective performance of TVAL3. Laser spot extraction and depth map estimation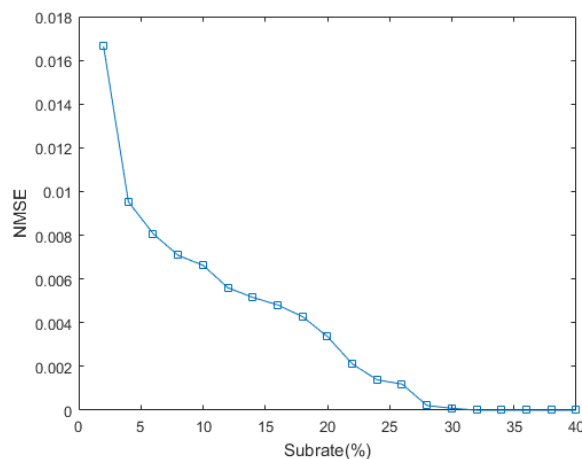 are proceeded along on the basis of the reconstructed intensity map. The quality of estimated depth map is getting better along with the subrate increase. With extremely low subrate in Fig. 4 (a) and (b), depth values of the pixels in the cardboards are not estimated correctly although it seems there are two boards in the target scene. With higher
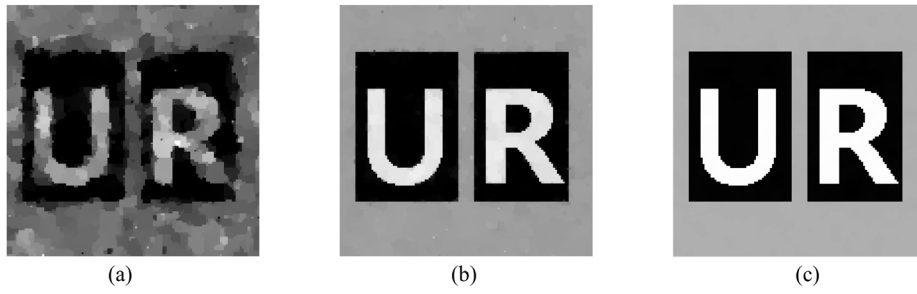
FIGURE 6. Visual comparison of the reconstructed intensity maps of the target scene by ISS with various subrates (from 4% to 12%) in the absence of noise. From left to right and top to bottom: the subrate increases successively by 4%.
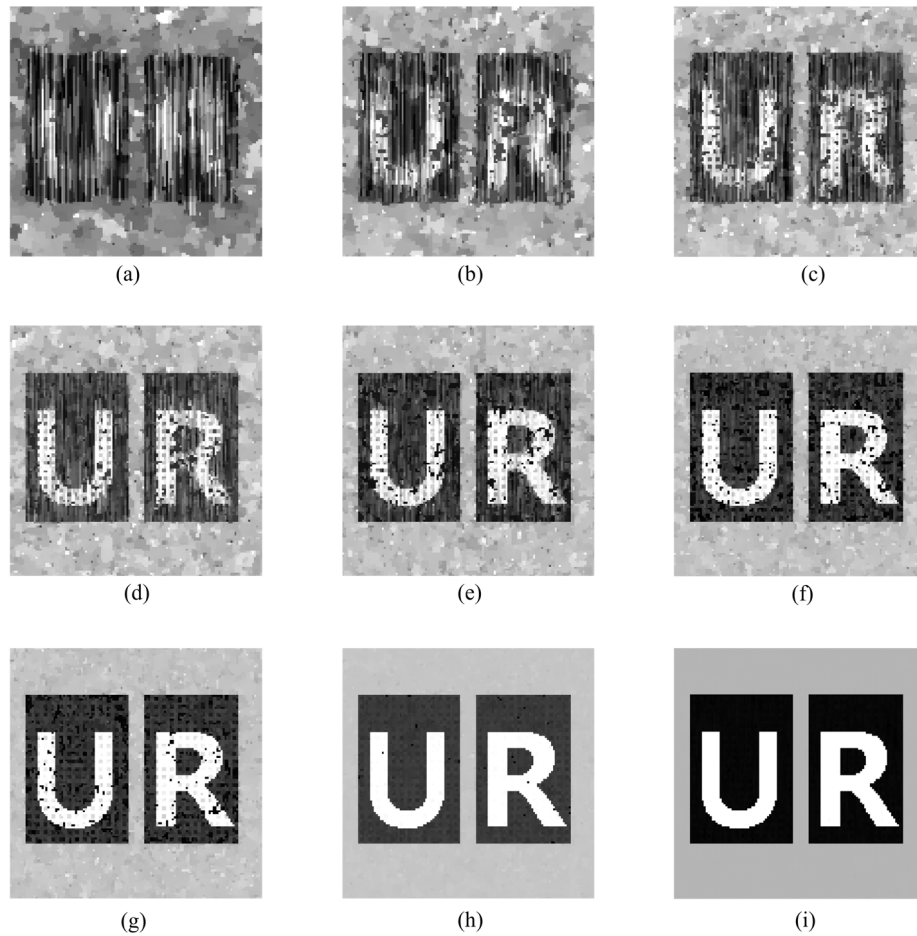

FIGURE 7. Visual comparison of the reconstructed intensity maps of the target scene by CSS with various subrates (from 4% to 40%) in the absence of noise. From left to right and top to bottom: the subrate increases successively by 4%.

subrate in Fig. 4 (c) – (f), only parts of the pixels in the cardboards are estimated with high accuracy and in the case of subrate greater than around 30% in Fig. 4 (g) – (i), accurate estimated depth maps are achieved. And then, a normalized mean squared error (NMSE) metric is adopted to compare the estimated depth maps with the original depth map [34].

$$NMSE = \frac{\sum_{i=1}^{n} \left(d(i) - \hat{d}(i) \right)^2}{\sum_{i=1}^{n} (d(i))^2} \qquad (14)$$

where $d(i)$ and $\hat{d}(i)$ are the depth of the ith pixel corresponding to the original depth maps and the estimated depth maps, respectively.

Fig. 5 provides a plot of NMSE as a function of subrates. It can be seen that the NMSE values decrease visibly when the subrates increase and accurate estimated depth maps are achieved after the subrate reaches 30%. From both subjective observation and objective evaluation, we can assert that the depth estimation method for the proposed prototype is effective.
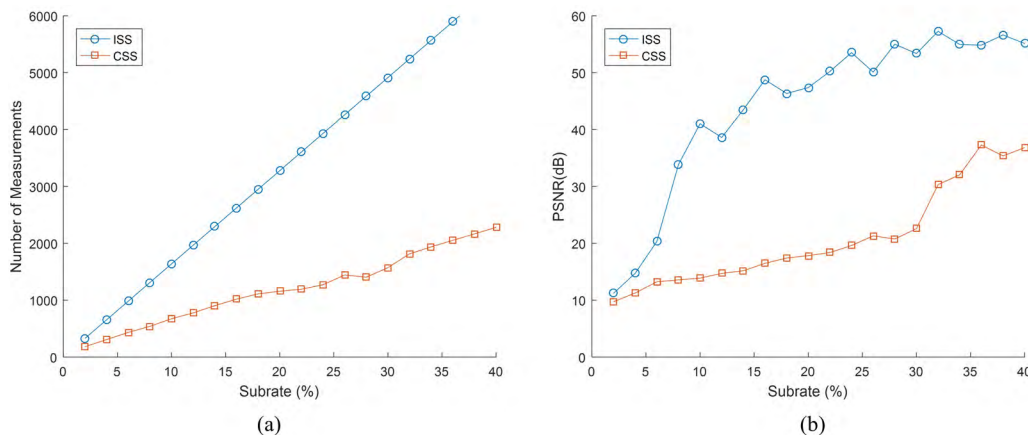
FIGURE 8. Comparison of PSNR and number of measurements between ISS and CSS. (a) Number of measurements as a function of subrates. (b) PSNR for reconstructed intensity maps as a function of subrates.

Fig. 6 is the visual comparison of the reconstructed intensity maps of the target scene by ISS. The sampling subrates varies from 4% to 12% as shown in Fig. 6 (a) to Fig. 6 (c). For the specific target consisted of square cardboards with letters, high-quality intensity map is obtained by ISS when the subrate is selected with equal or greater value of 8% in CS framework.

Fig. 7 is the visual comparison of the reconstructed intensity maps of the target scene by ISS. The sampling subrates varies from 6% to 34% as shown in Fig. 7 (a) to Fig. 7 (i). For the specific target consisted of square card-boards with letters, high-quality intensity map is obtained by ISS when the subrate is selected with equal or greater value of 30% in CS framework.

Fig. 8 compares the performance of two intensity reconstruction methods introduced in Section 4, integral sparse sampling and complementary sparse sampling. Fig. 8 (a) shows that the number of measurements to reconstruct intensity map of the target increases with increasing subrate for both the intensity reconstruction methods and the number is always greater when ISS is applied. The phenomenon, naturally, results from the fact that all of the pixels in the scene are considered as the target for ISS, but only the missed pixels for CSS. Fewer measurements and corresponding smaller size of measurement matrix can lead on to efficient engineering implementation and low-complexity computation. Fig. 8 (b) shows that the Peak Signal to Noise Ratio (PSNR) of the reconstructed intensity map of the target scene increases with increasing subrate for both intensity reconstruction methods and the number is always greater when ISS is applied. The quality of reconstructed intensity map by CSS is poor because a portion of the recovered pixels and the missed pixels for CSS are based on the results of the depth map estimation which are not good enough with lower subrates. The two figures show the trade-off between number of measurements, quality of recovered intensity maps and size of measurement matrixes.

TABLE 2. Performance of several CS-based 3D imaging methods.

Imaging method	Number of required frames	Required pulse width	Required sampling frequency
CS-TOF	2	≤ 2 ns	1 GHz or higher
CS-TS	dozens	> 2 ns	1 GHz or higher
proposed	2	free	pulse width related

Table 2 is provided for comparison with the performance of several CS-based 3D imaging methods. The main aim of 3D imaging is a achieving the range resolution of 0.3 m, as is shown in the simulation results above. Compared with conventional methods, the proposed method can obtain specific resolution without significantly increased numbers of acquired frames. More than that, the required width of the transmitting laser pulses and the required sampling frequency of the detector are irrelevant to the range resolution, which means that the proposed method can achieve range super-resolution to reconstruct the range-intensity profile free from the previous limitation of narrow-bandwidth pulsed lasers and high-frequency sampling.

VI. CONCLUSION
In this paper, we have presented a compressive sensing-based pulse-width-free LIDAR prototype that uses dual illumination, including a uniform illumination and a structured illumination for nonscanning 3D imaging to overcome the limitation of traditional methods. A 2D Dammann grating is applied to generate structured light in the form of diffractive spot matrix with equal intensity. Depth map of the target is obtained by recovering the distribution matrix of diffractive spot in CS framework. Intensity map of the target is obtained by integral sparse sampling under the proposed prototype. Alternately, it can be achieved by complementary sparse sampling as a trade-off between PSNR and the size of measurement matrix. Finally, the range-intensity profile of a 3D

scene is achieved as a combination of the estimated depth map and the reconstructed intensity map. The simulation results demonstrate that the proposed prototype is able to achieve a high-quality range-intensity profile of a 3D scene. In special, it has the advantage of range super-resolution when TOF LIDAR fails, i.e. echo pulses from targets with different ranges are indistinguishable. Beyond the simulations, building a realizable dual illumination system and using for 3D imaging to identify natural targets are future tasks.

ACKNOWLEDGMENT

REFERENCES

[1] P. F. McManamon, "Review of ladar: A historic, yet emerging, sensor technology with rich phenomenology," *Opt. Eng.*, vol. 51, no. 6, Jun. 2012, Art. no. 060901.

[2] P. Zhang, X. Du, J. Zhao, Y. Song, and H. Chen, "High resolution flash three-dimensional LIDAR systems based on polarization modulation," *Appl. Opt.*, vol. 56, no. 13, pp. 3889–3894, May 2017.

[3] R. Tobin *et al.*, "Long-range depth profiling of camouflaged targets using single-photon detection," *Opt. Eng.*, vol. 57, no. 3, Mar. 2018, Art. no. 031303.

[4] M. P. Edgar, S. Johnson, D. B. Phillips, and M. J. Padgett, "Real-time computational photon-counting LiDAR," *Opt. Eng.*, vol. 57, no. 3, Mar. 2018, Art. no. 031304.

[5] F. H. Xu *et al.*, "Revealing hidden scenes by photon-efficient occlusion-based opportunistic active imaging," *Opt. Express*, vol. 26, no. 8, pp. 9945–9962, Apr. 2018.

[6] B. Shi, Q. Lian, S. Chen, and X. Fan, "SBM3D: Sparse regularization model induced by BM3D for weighted diffraction imaging," *IEEE Access*, vol. 6, pp. 46266–46280, 2018.

[7] X. Zhang, C. Li, Q. Meng, S. Liu, Y. Zhang, and J. Wang, "Infrared image super resolution by combining compressive sensing and deep learning," *Sensors*, vol. 18, no. 8, p. 2587, Aug. 2018.

[8] M. F. Duarte and R. G. Baraniuk, "Kronecker compressive sensing," *IEEE Trans. Image Process.*, vol. 21, no. 2, pp. 494–504, Feb. 2012.

[9] L. P. Yaroslavsky, "Can compressed sensing beat the Nyquist sampling rate?," *Opt. Eng.*, vol. 54, no. 7, Feb. 2015, Art. no. 079701.

[10] E. J. Candès and M. B. Wakin, "An introduction to compressive sampling," *IEEE Signal Process. Mag.*, vol. 25, no. 2, pp. 21–30, Mar. 2008.

[11] D. L. Donoho, "Compressed sensing," *IEEE Trans. Inf. Theory*, vol. 52, no. 4, pp. 1289–1306, Apr. 2006.

[12] M. F. Duarte *et al.*, "Single-pixel imaging via compressive sampling," *IEEE Signal Process. Mag.*, vol. 25, no. 2, pp. 83–91, Mar. 2008.

[13] M. Rani, S. Dhok, and R. Deshmukh, "A systematic review of compressive sensing: Concepts, implementations and applications," *IEEE Access*, vol. 6, pp. 4875–4894, 2018.

[14] M.-J. Sun *et al.*, "Single-pixel three-dimensional imaging with time-based depth resolution," *Nat. Commun.*, vol. 7, Jul. 2016, Art. no. 12010.

[15] S. Foix, G. Alenya, and C. Torras, "Lock-in time-of-flight (ToF) cameras: A survey," *IEEE Sensors J.*, vol. 11, no. 9, pp. 1917–1926, Sep. 2011.

[16] G. A. Howland, D. J. Lum, M. R. Ware, and J. C. Howell, "Photon counting compressive depth mapping," *Opt. Express*, vol. 21, no. 20, pp. 23822–23837, Jan. 2013.

[17] G. A. Howland, P. B. Dixon, and J. C. Howell, "Photon-counting compressive sensing laser radar for 3D imaging," *Appl. Opt.*, vol. 50, no. 31, pp. 5917–5920, 2011.

[18] F. Li *et al.*, "CS-ToF: High-resolution compressive time-of-flight imaging," *Opt. Express*, vol. 25, no. 25, pp. 31096–31110, Dec. 2017.

[19] L. Li, L. Wu, X. Wang, and E. Dang, "Gated viewing laser imaging with compressive sensing," *Appl. Opt.*, vol. 51, no. 14, pp. 2706–2712, 2012.

[20] H. Gao, Y. Zhang, and H. Guo, "Multihypothesis-based compressive sensing algorithm for nonscanning three-dimensional laser imaging," *IEEE J. Sel. Topics Appl. Earth Observat. Remote Sens.*, vol. 11, no. 1, pp. 311–321, Jan. 2018.

[21] W. Xinwei, L. Youfu, and Z. Yan, "Multi-pulse time delay integration method for flexible 3D super-resolution range-gated imaging," *Opt. Express*, vol. 23, no. 6, pp. 7820–7831, 2015.

[22] H. Dammann and K. Görtler, "High-efficiency in-line multiple imaging by means of multiple phase holograms," *Opt. Commun.*, vol. 3, no. 5, pp. 312–315, Jul. 1971.

[23] J. Zhang, C. Zhou, and X. Wang, "Three-dimensional profilometry using a Dammann grating," *Appl. Opt.*, vol. 48, no. 19, pp. 3709–3715, Jul. 2009.

[24] S. Wei, C. Zhou, S. Wang, K. Liu, X. Fan, and J. Ma, "Colorful 3-D imaging using an infrared Dammann grating," *IEEE Trans. Ind. Inform.*, vol. 12, no. 4, pp. 1641–1648, Aug. 2016.

[25] S. Wei, S. Wang, C. Zhou, K. Liu, and X. Fan, "Binocular vision measurement using Dammann grating," *Appl. Opt.*, vol. 54, no. 11, pp. 3246–3251, Apr. 2015.

[26] W. R. Babbitt, Z. W. Barber, and C. Renner, "Compressive laser ranging," *Opt. Lett.*, vol. 36, no. 24, pp. 4794–4796, 2011.

[27] C. F. Caiafa and A. Cichocki, "Multidimensional compressed sensing and their applications," *Wiley Interdiscipl. Rev., Data Mining Knowl. Discovery*, vol. 3, no. 6, pp. 355–380, 2013.

[28] J. Romberg, "Imaging via compressive sampling," *IEEE Signal Process. Mag.*, vol. 25, no. 2, pp. 14–20, Mar. 2008.

[29] J. Fade, E. Perrotin, and J. Bobin, "Polarizer-free two-pixel polarimetric camera by compressive sensing," *Appl. Opt.*, vol. 57, no. 7, pp. B102–B113, Mar. 2018.

[30] L. H. Bian, J. L. Suo, Q. H. Dai, and F. Chen, "Experimental comparison of single-pixel imaging algorithms," *J. Opt. Soc. Amer. A*, vol. 35, no. 1, pp. 78–87, Jan. 2018.

[31] H. Gao, Y.-M. Zhang, and H.-C. Guo, "A compressive sensing algorithm using truncated SVD for three-dimensional laser imaging of space-continuous targets," *J. Mod. Optic.*, vol. 63, no. 21, pp. 2166–2172, May 2016.

[32] A. Kirmani, A. Colaço, F. N. Wong, and V. K. Goyal, "Exploiting sparsity in time-of-flight range acquisition using a single time-resolved sensor," *Opt. Exp.*, vol. 19, no. 22, pp. 21485–21507, 2011.

[33] A. Colaço, A. Kirmani, G. A. Howland, J. C. Howell, and V. K. Goyal, "Compressive depth map acquisition using a single photon-counting detector: Parametric signal processing meets sparsity," in *Proc. IEEE Conf. Comput. Vis. Pattern Recognit.*, Jun. 2012, pp. 96–102.

[34] N. Gopalsami *et al.*, "Passive millimeter-wave imaging with compressive sensing," *Opt. Eng.*, vol. 51, no. 9, Sep. 2012, Art. no. 091614.

YULONG AN received the B.S. degree in information engineering from the Beijing Institute of Technology, Beijing, China, in 2011, where he is currently pursuing the Ph.D. degree. His research interests include laser imaging and compressive sensing.

YANMEI ZHANG received the B.S. degree in electromechanical engineering, the M.S. degree in mechanical and electrical automation, and the Ph.D. in electromechanical engineering from the Beijing Institute of Technology, in 1989, 1995, and 2010, respectively.

Since 1995, she has been with the School of Information and Electronics, Beijing Institute of Technology, as a Professor and a Ph.D. Supervisor. Her research interests include signal detection, signal processing technology, photoelectric detection, and imaging processing technology.

HAICHAO GUO received the B.S. degree in optical engineering from the University of Electronic Science and Technology, in 2006, and the M.S. degree in electrical engineering from the University of Chinese Academy of Sciences, in 2009. Since 2009, he has been with the National Key Laboratory of Science and Technology on Space Microwave and with the School of Information and Electronics, Beijing Institute of Technology, studying satellite free space coherent optical communication and laser imaging.

JING WANG received the B.S. degree in electronic information engineering from the Nanjing University of Science and Technology, in 2017. She is currently pursuing the master's degree with the Beijing Institute of Technology, Beijing, China. Her research interests include laser imaging and compressive sensing.

• • •